JOURNAL OF MORPHOLOGY 268:284–292 (2007)

Quantification of Red Myotomal Muscle Volume and Geometry in the Shortfin Mako Shark (*Isurus oxyrinchus*) and the Salmon Shark (*Lamna ditropis*) using T_1-weighted Magnetic Resonance Imaging

Cameron N. Perry,[2] Daniel P. Cartamil,[4] Diego Bernal,[5] Chugey A. Sepulveda,[6] Rebecca J. Theilmann,[2] Jeffrey B. Graham,[4] and Lawrence R. Frank[1,2,3]*

[1]*Center for Scientific Computation in Imaging, University of California, San Diego, La Jolla, California 92093*
[2]*Center for Functional Magnetic Resonance Imaging, University of California, San Diego, La Jolla, California 92093*
[3]*VA San Diego Health Care System, San Diego, California 92161*
[4]*Marine Biology Research Division and Center for Marine Biotechnology and Biomedicine, Scripps Institution of Oceanography, University of California, San Diego, La Jolla, California 92093-0204*
[5]*Department of Biology, University of Massachusetts, Dartmouth, Dartmouth, Massachusetts 02747*
[6]*Pfleger Institute of Environmental Research, Oceanside, California 92054*

ABSTRACT T_1-weighted magnetic resonance imaging (MRI) in conjunction with image and segmentation analysis (i.e., the process of digitally partitioning tissues based on specified MR image characteristics) was evaluated as a noninvasive alternative for differentiating muscle fiber types and quantifying the amounts of slow, red aerobic muscle in the shortfin mako shark (*Isurus oxyrinchus*) and the salmon shark (*Lamna ditropis*). MRI-determinations of red muscle quantity and position made for the mid-body sections of three mako sharks (73.5–110 cm fork length, FL) are in close agreement (within the 95% confidence intervals) with data obtained for the same sections by the conventional dissection method involving serial cross-sectioning and volumetric analyses, and with previously reported findings for this species. The overall distribution of salmon shark red muscle as a function of body fork length was also found to be consistent with previously acquired serial dissection data for this species; however, MR imaging revealed an anterior shift in peak red muscle cross-sectional area corresponding to an increase in body mass. Moreover, MRI facilitated visualization of the intact and anatomically correct relationship of tendon linking the red muscle and the caudal peduncle. This study thus demonstrates that MRI is effective in acquiring high-resolution three-dimensional digital data with high contrast between different fish tissue types. Relative to serial dissection, MRI allows more precise quantification of the position, volume, and other details about the types of muscle within the fish myotome, while conserving specimen structural integrity. J. Morphol. 268:284–292, 2007.

KEY WORDS: magnetic resonance imaging; tissue segmentation; red muscle volume; mako shark; salmon shark; myotome anatomy

The ability to distinguish the two major muscle types (i.e., the aerobic, slow twitch red muscle and the glycolytic, fast-twitch white muscle) in the myotomes of fishes is of key importance in understanding specializations in morphology, locomotion, and physiology (Graham et al., 1983; Carey et al., 1985; Shadwick et al., 1999; Ellerby et al., 2000; Bernal et al., 2003; Donley et al., 2004; Sepulveda et al., 2005). Fishes of particular interest in this respect include the tunas (Scombridae) and lamnid sharks (Lamnidae) in which a unique anterior and medial position of red muscle within the body myotome is one of several specializations contributing to a capacity for regional endothermy (elevation of red muscle temperature above that of ambient water) (Carey and Teal, 1969; Carey et al., 1971; Graham and Dickson, 2001; Bernal et al., 2001a; Bernal et al., 2003) and utilization of the unique thunniform swimming mode (Graham and Dickson, 2004; Shadwick, 2005).

Past studies of fish muscular anatomy have most often utilized the conventional method of serial, transverse sectioning of the entire specimen followed by the dissection, removal, and either the weighing (Graham et al., 1983) or estimation of mass by volume displacement (Woodhead et al., 2001) of the tissue or muscle groups of interest within each section. Or, as an option to volume displacement, the surface area of each tissue in

Contract grant sponsor: NSF; Contract grant number: DBI-0446389; Contact grant sponsor: California Sea Grant; Contract grant number: RF-193; Contact grant sponsor: UCSD Academic Senate.

*Correspondence to: Lawrence R. Frank, Center for Scientific Computation in Imaging, UCSD, 9500 Gilman Dr no. 0854, La Jolla, Ca 92093-0854. E-mail: lfrank@ucsd.edu

Published online 13 February 2007 in
Wiley InterScience (www.interscience.wiley.com)
DOI: 10.1002/jmor.10516

each section could be calculated using photographs of the cut surface, followed by mathematical extrapolation of tissue volume by multiplying the surface area by slice thickness. Photography often aids quantitative morphological descriptions of red muscle in relation to structural features such as the vertebral column and position along the body axis (Bernal et al., 2003; Graham and Dickson, 2004; Sepulveda et al., 2005).

However, serial sectioning and dissection have several disadvantages. One of these is the assumption that objective, visual distinction of different muscle types for dissection will be possible, which is not always the case. Further, elucidation of anatomical detail through careful dissection is extremely labor intensive and, because cutting the specimen can introduce distortions due to shear and tearing, even the best dissections seldom offer the possibility of reconstructing the specimen to visualize basic design features of the intact, three-dimensional (3D) state. Finally, dissection usually results in nearly complete destruction of specimens, precluding further analysis and making work on rare and valuable material problematic.

One alternative method to serial dissection is magnetic resonance imaging (MRI), a noninvasive 3D radiographic modality particularly well-suited for the imaging of soft tissues including muscle (Kirschner-Hermanns et al., 1997; Hodgson et al., 2006). An earlier MRI study on sharks (Waller et al., 1994) demonstrated its capacity to qualitatively contrast images of cartilage and various soft tissues including brain, digestive tract, and muscle. The objective of the present study is to evaluate the relative effectiveness of MRI and segmentation analysis (the process of digitally partitioning tissues based upon specific MR image characteristics) in quantifying red muscle position and volume in two species of lamnids, the mako (*Isurus oxyrinchus*) and the salmon shark (*Lamna ditropis*). This evaluation entails the comparison of results obtained by MRI with results obtained, for the same material, by conventional dissection, and the comparison of the red muscle data obtained by both of these methods with red muscle data recently published for the mako and salmon sharks (Bernal et al., 2003).

MRI SYNOPSIS

MRI is based on the signals generated by water molecules from radio-frequency (RF) excitation while immersed in a large static magnetic field, combined with additional, smaller, spatially varying magnetic fields that produce localized variations in these signals. It provides a complementary approach to other imaging methods such as computed tomography (CT), which uses X-rays and thus distinguishes tissues on the basis of density. Differences in the amount and states of water within the tissues are manifest as alterations in the MR signal and can be accentuated by altering the parameters of the MR acquisition (i.e., echo time, flip angle) to provide image contrast between tissues of different types. MRI can acquire fully 3D data at user-defined resolutions (Frank, 2002). The individual volume resolution elements, or voxels, are often chosen to be cubical in high resolution studies such as the present one to facilitate accurate measurements during postprocessing.

Two MR signal parameters that are particularly useful for distinguishing different tissues are the rate at which the RF-excited signal decays, and rate at which thermal equilibrium is restored to the sample within the large, static field, following excitation. Both of these signal changes are characterized by simple exponential functions. The rate of thermal equilibrium restoration is characterized by the parameter T_1 according to $(1\text{-}\exp(t/T_1))$. The RF signal decay as a function of time t is characterized by the decay rate T_2, as $\exp(-t/T_2)$. Because of differences in their microstructure, tissues have different intrinsic T_1 and T_2 values and can be distinguished on this basis (Frank, 2002). Image contrast between different tissues is done by accentuating T_1 and T_2 differences through manipulation of the user-controlled parameters of the MR image acquisition. Emphasizing T_2 variations, called "T_2-weighted imaging," is useful in distinguishing between tissue and fluids. T_1-weighted imaging is a standard way in which to distinguish different tissues (Kirschner-Hermanns et al., 1997) including muscle (Bonney et al., 1998) and is the method used in the current study. Once these are acquired, the data can be digitally partitioned into virtual, 3D objects whose location and geometry (including volumes, cross-sectional areas, relative orientation) can be quantitatively assessed.

MATERIALS AND METHODS

Mako Shark

Three juvenile shortfin mako sharks (*Isurus oxyrinchus*) (fork length [FL] 73.5 cm [3.8 kg body mass], 99 cm [9.7 kg body mass], and 110 cm [13.5 kg body mass]) were captured off the coast of southern California using methods described by Bernal et al. (2001b), and approved by the Institutional Animal Care and Use Committee, University of California, San Diego. Following the use of these specimens in other experimental studies (Bernal et al., 2001b), they were euthanized and frozen whole until MRI analysis was performed. Prior to imaging, specimens were thawed and a large section was removed from the mid-body region, beginning anterior to the first dorsal fin (41–42% FL) and ending behind it (61–68% FL).

Axial MRI data were acquired for each mako body section using a 1.5 Tesla GE Signa Clinical scanner (GE Healthcare, Milwaukee, WI) with a standard knee RF receive coil. Data were collected using a T_1-weighted 3D spoiled gradient recalled echo acquisition with the following parameters: 50° flip angle, 60.0 ms repetition time, 5.0 ms echo time, and 16 kHz bandwidth. For each specimen, images were acquired at a fixed slice thickness (0.15 cm) and in-plane area (field-of-view, FOV). The FOV of each acquisition was adjusted to encompass the maximum transverse sectional area of each specimen order to maximize the resolution. The respective number of slices, FOV, and total scan times for

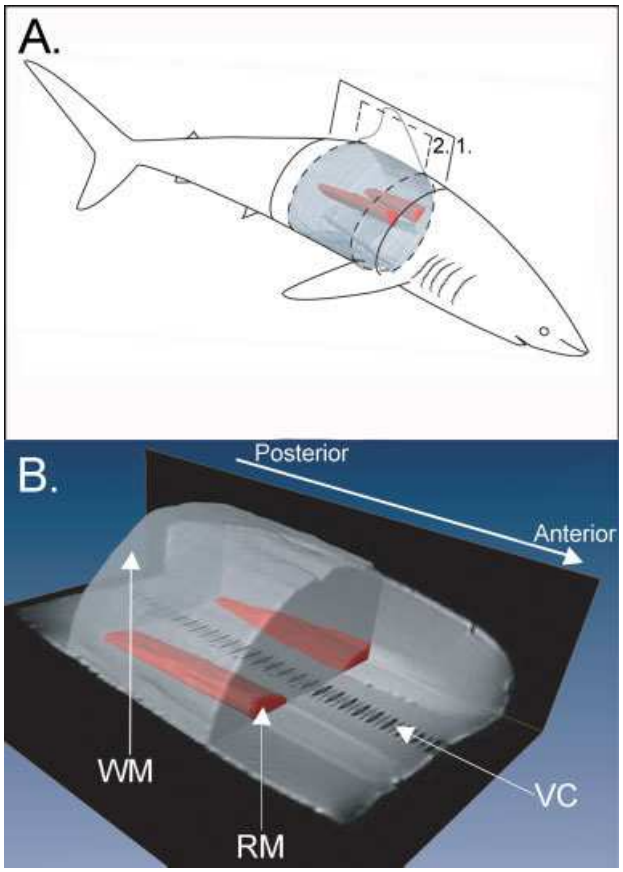

Fig. 1. **A**: Three-dimensional illustration of a mako shark (*Isurus oxyrinchus*) with an overlay showing the body section that was scanned and volumetrically analyzed by MRI along with the position of the right and left red muscle (RM) loins (red). Section inside bracket 1 (solid line) represents the entire body region removed for MRI analysis. Section encompassed by bracket 2 (dashed line) represents the segment resolved by MRI and by subsequent dissection (see text). **B**: Three-dimensional, anterior-sagittal perspective, obtained by MRI and segmentation analysis, showing red muscle position relative to the vertebral column (VC) in a 13-cm long mid-body segment of a mako shark. Other symbols: WM, white muscle.

each specimen were as follows: 73.5 cm FL: 64 slices, 20 cm FOV, 526 s scan time; 99 cm FL: 110 slices, 26 cm FOV, 879 s; and 110 cm FL: 104 slices, 22 cm FOV, 833 s. One of these imaged volumes is shown in Figure 1A within the correct anatomical context. Figure 1B shows a digitally cut section of the imaged volume in Figure 1A with the major anatomical components.

Data were processed using the Amira software program (Mercury Computer Systems, Berlin, Germany) and two different analyses, red muscle fractional volume estimation by tissue segmentation, and red muscle position relative to the vertebral column, were performed. For both analyses, data were interpolated by a factor of two in each dimension and a 3D Lanczos filter was employed to enhance tissue boundaries and sharpen edge detail by reducing aliasing. Segmentation analysis differentiated the volumes of two tissue groups, red muscle and non-red muscle tissues (i.e., all other nonvisceral tissues including white muscle, skin, connective tissue, and vertebrae) in the body segment on the basis of their intrinsic T_1-weighted image intensities. Because of tissue damage along the cut edges and MRI signal attenuation due to fall off of the receiver coil sensitivity, segmentation analysis could not be performed to the extent of the anterior and posterior ends of each body section. The segmented data were then smoothed using a modified Gauss filter and virtual 3D models of the red muscle and the non-red muscle components generated. These were used to calculate red muscle and non-red muscle volumes and relative red muscle cross-sectional areas (defined as the ratio of red muscle to total body volume at a specific FL to that at 50% FL). The relative volumes of the red muscle and non-red muscle tissues determined for each body section were compared with values obtained within the same section by dissection. Findings for the axial distribution of red muscle cross-sectional area were compared to values in Bernal et al. (2003).

From axial image planes, the distance (D_{mv}) between RM and the vertebral column was determined at five different positions (45–65% FL, in 5% FL increments) along the body axis. These data were used to calculate the *relative red muscle-vertebral column distance* D_{rel}, which is D_{mv} at any point z along the fish length, divided by D_{mv} at 50% FL.

Dissection

Red muscle quantity was determined by dissection of serial transverse sections of each shark body section. The section of each fish that was dissected spanned 45–65% FL and had the same dimensions as the section imaged by MRI and processed by segmentation analysis (Fig. 1A). Red muscle was dissected by making a longitudinal incision at the base of the dorsal fin and advancing ventrally through the white muscle until reaching the surrounding connective tissue. The red muscle was then extracted and water displacement volume estimates (Woodhead et al., 2001) were made for red muscle and nonred muscle. The volume fraction of red muscle (RM%) was then calculated. Because both the MRI and dissection determinations of volume were made on the same section, direct comparisons of the results could be made on a per-specimen basis.

Salmon Shark

A juvenile female salmon shark (*Lamna ditropis*), FL 81.5 cm (9.0 kg body mass), made available shortly after washing ashore at Bodega Bay, CA, afforded us the uncommon opportunity to perform MRI-based measurements of the axial distribution and volume of red muscle in an intact specimen for comparison with previously obtained dissection measurements for this species (Bernal et al., 2003). Whole shark T_1-weighted MRI data were acquired over the entire length of the specimen on a 3.0T GE Excite clinical scanner using a Nova RF receive coil (Nova Medical, Inc., Wilmington, MA) set at the following parameters: transverse orientation, 3D fast spoiled gradient recall echo acquisition, 30° flip angle, minimum full echo time, 22 cm field of view, frequency 256, phase 256, 160 slices, 1.0 mm slice thickness, and 31.25 kHz bandwidth. Because the specimen was substantially longer than the receive coil, a sequence of five consecutive image volumes was acquired. These volumes were slightly overlapped to facilitate postprocessing image registration (the alignment of adjacent image volumes using landmarks) and Amira was used to produce one full-body dataset. Subsequent to MR imaging, serial dissection of the salmon shark was performed for validation of the segmentation analysis, particularly confirmation of the red muscle endpoint (i.e., the % FL where red muscle is no longer present).

RESULTS

Mako Shark

Figure 2 shows good agreement in red muscle volumes for the body sections of the three sharks determined by MRI with the corresponding region of the whole body red muscle data obtained by Bernal et al. (2003). The mean (±SD) relative red muscle cross-sectional areas at the five selected

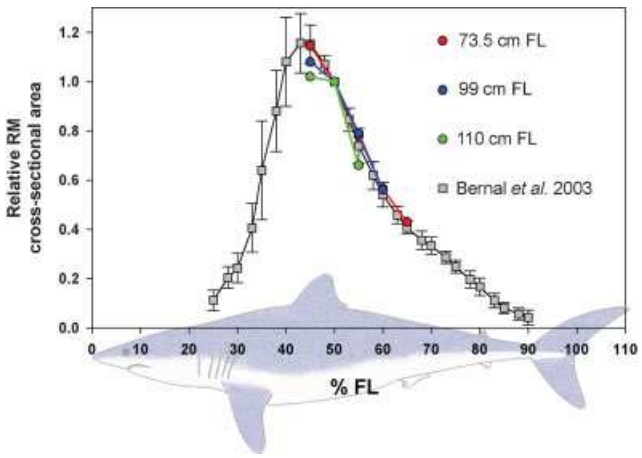

Fig. 2. MRI determined relative red muscle cross-sectional area estimates for the short body sections of three mako sharks (*Isurus oxyrinchus*) used in this study compared to the red muscle area vs. %FL relationship for whole mako sharks described by Bernal et al. (2003).

body positions were: 45% FL, 1.12 ± 0.02; 50% FL, 1.0; 55% FL, 0.74 ± 0.02; 60% FL, 0.55 ± 0.01; 65% FL, 0.44 ± 0.01. Each of these estimates occurs within the 95% confidence intervals of data obtained at the same body position in different mako specimens by Bernal et al. (2003). Results of MR-based and conventional volumetric analysis for the three mako sharks are shown in Table 1. No significant difference was found in the estimated red muscle volume per section determined by the two methods (paired *t*-test, $P = 0.18$). Figure 3A illustrates one axial image plane of a mako shark to show how D_{mv} was determined and Figure 3B shows that D_{rel} increases posteriorly. Values for D_{rel} at different body positions are: 45% FL, 0.90 ± 0.06; 50% FL, 1.0; 55% FL, 1.18 ± 0.07; 60% FL, 1.45 ± 0.01; 65% FL, 1.56.

Salmon Shark

The MRI-generated axial profiles of relative red muscle cross-sectional area in the 9.0 kg salmon shark are in general agreement with the previously published serial dissection and digital photographic results for larger salmon sharks examined by serial dissection (Bernal et al., 2003) and these comparisons are shown in Figure 4. While the approximate point of red muscle origin for all three sharks is similar (21–25% FL), curves for the larger sharks indicate an anterior shift in the position of maximum red muscle cross-sectional area, suggesting that red muscle mass is added to the anterior body region as size increases. The posterior extension of red muscle is in two loins lateral to the vertebral column that taper to an endpoint where red muscle is no longer discernible. However, MRI (see Fig. 4) showed a more protracted red muscle endpoint (i.e., it appears to extend further down the body, Fig. 4) relative to the red muscle endpoints indicated by Bernal et al. (2003). Subsequent serial dissections (see Fig. 5) confirmed, in close agreement with the findings of Bernal et al. (2003), that the red muscle endpoint of the 9.0 kg *Lamna ditropis* occurs between 61% FL and 64% FL (arrow in Fig. 4). The protracted endpoint seen in Figure 4 is due to hypaxial lateral tendon, which has a markedly similar MR image intensity to red muscle. This tendon forms along the median edge of the main anterior-pointing cone of myotomal muscle, and transmits force generated by red muscle posteriorly, thereby connecting red muscle to the skin in the region of the caudal peduncle. This tendon's appearance and linkage in the salmon shark are both similar to the hypaxial lateral tendon described for the mako shark (Shadwick, 2005). Serial MRI and dissection sections (see Fig. 5) detail the red muscle-lateral tendon transition and show the tendon's crescent shape, which reflects its origin in red muscle myosepta.

DISCUSSION

This study demonstrates the efficacy of MRI, along with image and segmentation analysis, in determining the location and volume of red muscle

TABLE 1. Comparison of the estimates, by MRI and segmentation analysis and by conventional dissection and water-displacement, for RM and body segment volumes obtained for the sections of three mako sharks (Isurus oxyrinchus)

			Analytical method					
			MRI-segmentation			Conventional		
FL (cm)	Mass (kg)[a]	Range (%FL)[b]	RM volume (cm^3)	Total segment volume (cm^3)[c]	Relative RM volume (%)[d]	RM volume (cm^3)	Total segment volume (cm^3)[c]	Relative RM volume (%)[d]
73.5	3.8	50–62	35.3	727.6	4.85	21.5	434.5	4.95
99.0	9.7	47–61	64.5	1335.7	4.83	72.0	1435.0	5.02
110	13.5	42–51	87.6	2070.4	4.23	69.0	1444.0	4.78

[a]Body mass estimated from fork length using values in Kohler et al. (1996).
[b]Indicates measured portion of the body.
[c]The entire volume of the body segment on which the RM volume estimate is based.
[d]% RM in the section estimated by: RM/(RM + body volume).

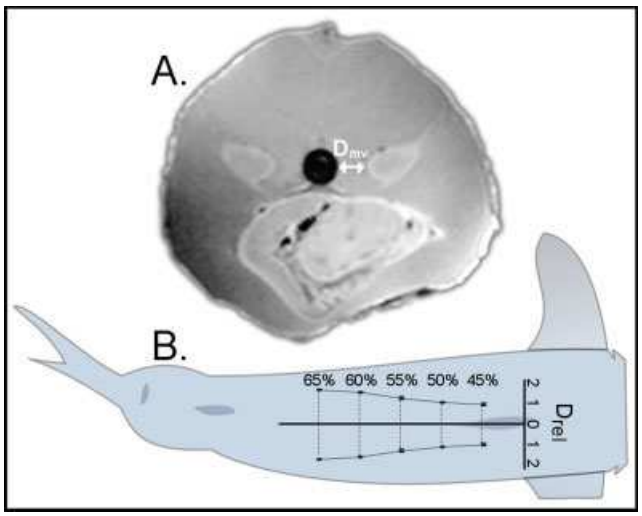

Fig. 3. **A**: Axial image plane for the mako shark (*Isurus oxyrinchus*) showing D_{mv}, the distance between the vertebral column (black circle) and the red muscle loin. **B:** Mako D_{rel} as a function of FL.

in lamnid sharks. Using MRI, the distinct and well-described morphological characteristics of red muscle and white muscle (Bone, 1978) could be contrasted on the basis of microstructure by T_1-weighted imaging. Our study presents quantitative data on red muscle volume and distribution and demonstrates close agreement between the MR-based findings and those obtained by dissection followed by either direct volumetric or digital transverse-sectional analyses.

Two new observations about salmon shark red muscle structure were revealed by this MRI study. The first of these is the apparent anterior shift in the axial position of maximum red muscle occurring in larger sharks relative to the 9.0 kg specimen (see Fig. 4). Additional studies are needed to understand the mechanism of this shift. Based on present data, the shift appears attributable to both the growth of red muscle as well as changes in body mass. Bernal et al. (2003) reported that in the mako, other lamnids, and the few other sharks they studied, the scaling of red muscle mass is directly proportional to body mass, and makos and salmon sharks both had a relative red muscle mass of 2%. Assuming a 2% relative red muscle mass, a salmon shark growing from 9 to 16 kg would increase its red muscle from 180 to 320 g. For sharks, as is the case for most organisms, mass increases as the cube of length (Kohler et al., 1996), which means that large changes in body girth occur with small changes in length. Further, length-mass comparison of the body length-mass relationships shows a markedly greater increase in mass for the salmon shark (Goldman and Music, 2006) than for the mako shark (Mollet et al., 2000). In the present study the 9.0 kg salmon shark had a fork length of 81.5 cm and thus a mass to fork length ratio of 0.11 kg cm^{-1}. The 15.9 kg salmon shark studied by Bernal et al. (2003) had a 105 cm fork length, and its mass to fork length ratio was 0.151 kg cm^{-1}.

The second observation was realized because the MR parameters used for imaging were not pre-set to distinguish between red muscle and the lateral tendon and resulted in images initially suggesting a longer protracted red muscle in the 9.0 kg salmon shark (see Fig. 4). Because this finding did not agree with the results of Bernal et al. (2003), the terminal red muscle region of the salmon shark was dissected for confirmation and this revealed additional detail for red muscle-hypaxial lateral tendon transition (see Fig. 5). Future studies could use adjusted MRI parameters to generate images having good muscle-tendon contrast, and thus allow comparative studies of the force transmission systems of different lamnids. Also important for further study are comparisons of lamnids and tunas, which are markedly convergent for both the position of red muscle deep within the myotomes near the vertebral column and relatively anterior in the body, as well as the arrangements of the tendons that transmit force from the red muscle to the caudal region (Bernal et al., 2001a, 2003; Donley et al., 2005).

The potential importance of comparative MRI analysis to the physiology and functional morphology of lamnids and other species is illustrated by Figure 6, which shows the full-body MRI scan of the salmon shark and contrasts the red muscle positions in the salmon and mako sharks. The MR image in Figure 6A shows the parallel left and

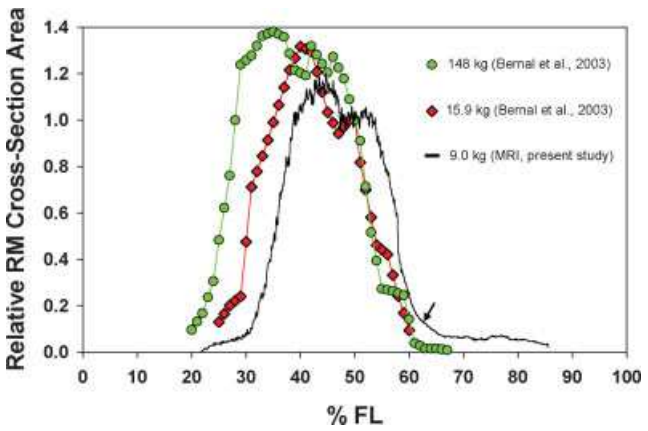

Fig. 4. Comparisons of red muscle quantity and position in three differentially sized salmon sharks (*Lamna ditropis*), showing the anterior shift in red muscle in larger sharks. Data for the 9 kg shark were obtained from whole-body MRI images. The arrow indicates the transition region between the red muscle and tendon. Data for the 15.9 and 148 kg specimens were obtained by serial sectioning and dissection (Bernal et al., 2003).

right red muscle loins of the salmon shark extending from near the rostrum to approximately 61% FL. Body profiles of the two sharks (Fig. 6B) show the thicker body of the salmon shark relative to the mako (Mollet et al., 2000; Goldman and Music, 2006) as well as the salmon shark's shorter red muscle end point (61 vs. 90% fork length; Bernal et al., 2003). In both the mako and the salmon shark, lateral tendons emanate from each myotome along the entire span of the red muscle and proceed posteriorly to their point of insertion into the skin in the region of the caudal peduncle. Accordingly, differences in the red muscle end points thus have the potential to affect tendon length and swimming kinematics. Bernal et al. (2003), for example, suggested that the more anterior end point of salmon shark red muscle likely results in a more rigid swimming mode than occurs in the mako. Kinematic studies on the mako verify its thunniform swimming mode (i.e., minimum lateral displacement of the anterior body) and show that pronounced lateral displacement of the posterior body (i.e., the bending point) begins at approximately 60% total body length (Donley et al., 2005; Shadwick, 2005). No kinematics data exist for the salmon shark and would be important in evaluating how differences in the red muscle-tendon linkages affect body stiffness and caudal oscillation in the two sharks.

The need to maintain an elevated temperature in the red muscle and other tissues is another functional difference that appears strongly related to the different positions of red muscle in the salmon and mako sharks. The salmon shark, which occurs in the northern Pacific Ocean waters often as cool as 6°C, has red muscle temperatures that may be as warm as 26°C (Anderson and Goldman, 2001; Bernal et al., 2005). It has a more extreme heat-conservation challenge than does the mako shark, which occurs in sub-temperate to tropical regions (Compagno, 2001). The vascular retia (counter-current heat exchangers) bounding the arterial and venous blood supply to red muscle are the most effective mechanism for lamnid heat conservation. Reflecting the much larger thermal gradient between red muscle and ambient water experienced by the salmon shark is its greater

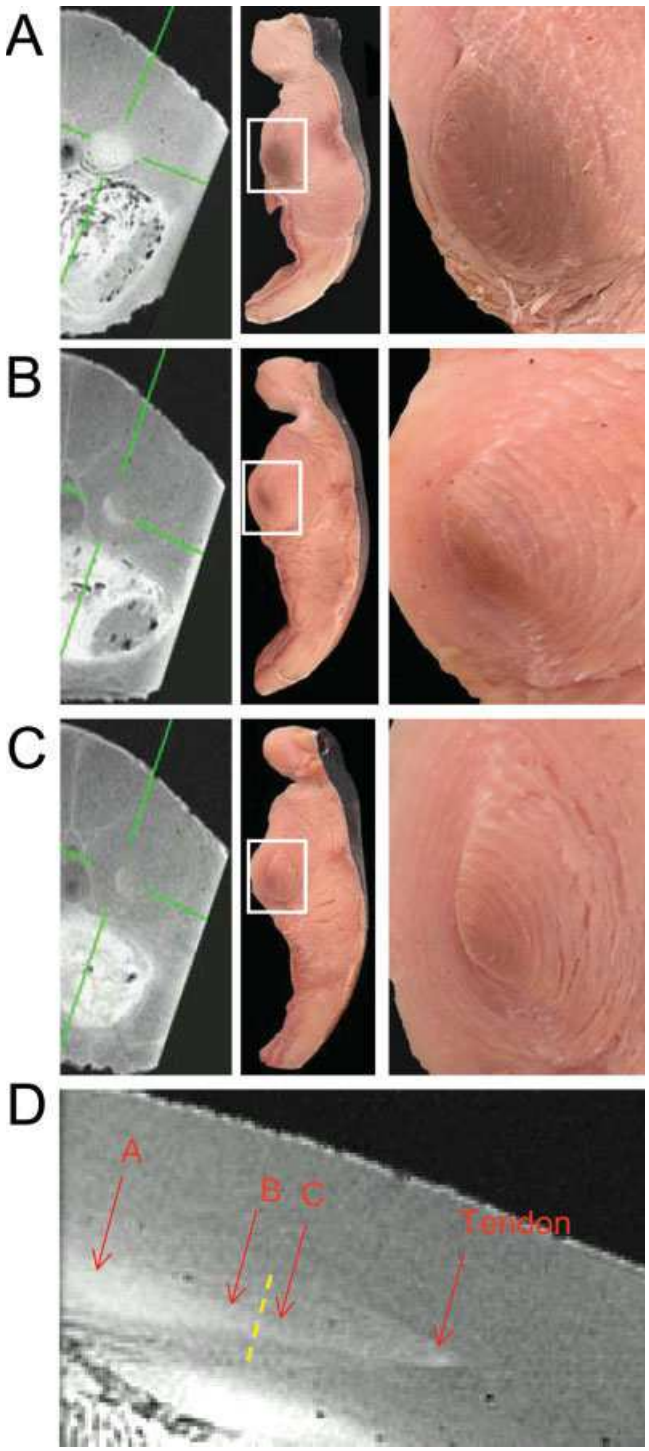

Fig. 5. MR and digital camera images of the left-side myotome and red muscle loin in the 9.0 kg (81.5 cm FL) *Lamna ditropis* at three body positions (**A**) 51% FL, (**B**) 61% FL, and (**C**) 64% FL. Note that red muscle is present at 61% FL but only the hypaxial lateral tendon is present at 64% FL. Left: MRI scans showing (between the green crosshairs) the transition between red muscle and the hypaxial lateral tendon. **A:** Red muscle is an ellipsoid. **B:** Crescent shaped red muscle mass just anterior to the tendon. **C:** Crescent of the tendon after the red muscle endpoint. Center: Digital camera images of dissected filets at the same locations of A–C in left column. Indentations above and below the red muscle are sites of the removed vertebrae (above) and the empty coelom (below). MR images are scaled to fill the frame of the figure. Right: Close-up views of tissue outlined in white boxes in center column. **D:** Sagittal section through the body showing positions of A, B, and C above. Anterior of the body is to the left. Vertical dashed line marks the approximate endpoint of the red muscle, and corresponds to the arrow in Figure 4. The tendon can be seen posterior to the dashed line. The high-intensity region below red muscle is the coelomic cavity.

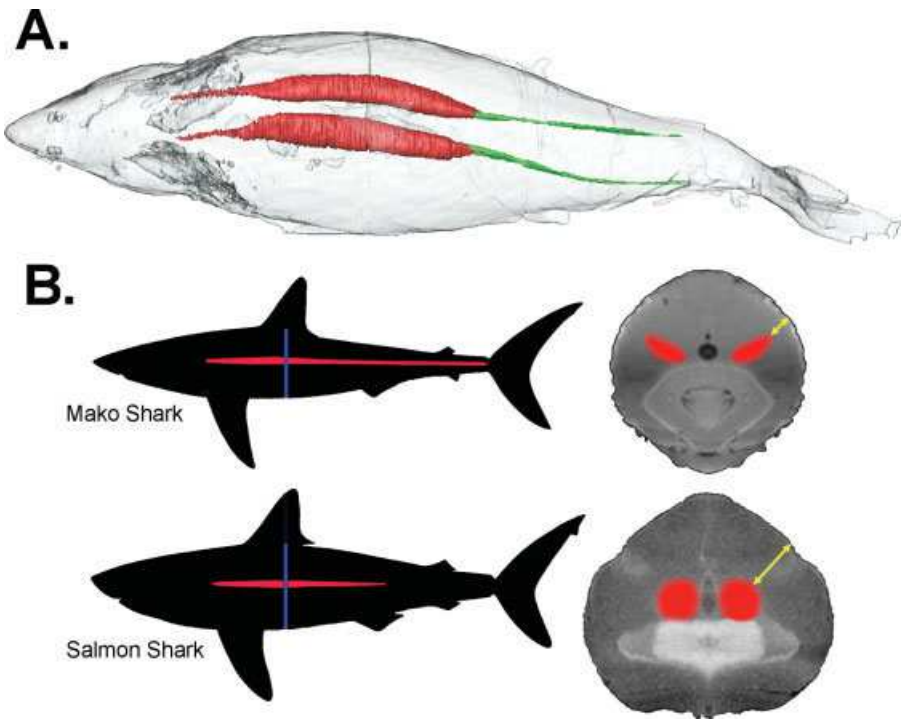

Fig. 6. **A:** Whole-body MR image of the 9.0 kg (81.5 cm FL) salmon shark (*Lamna ditropis*), showing the paired red muscle loins (red) and the hypaxial lateral tendons (green) extending from red muscle to the caudal keel. **B:** (Left) Lateral profiles comparing the body forms of a mako (*Isurus oxyrinchus*) and a salmon shark having similar total length, and showing the relative position and extent of red muscle in each. The bulk of the salmon shark's red muscle (red) is contained within the central body region, which is thicker than that of the mako shark. In contrast, mako red muscle extends to 90% total length. [Shark profiles modified from Ebert, 2003]. B: (Right) Comparison of axial cross sections of mako and salmon sharks, taken at 40% total length (blue vertical lines in body profiles), showing the greater relative distance (denoted by yellow arrows) between red muscle and the body perimeter. Expressed as a percentage of total body width, these distances are 13.5% for the mako, and 22% for the salmon shark.

number of vessel rows (60–69) comprising the lateral retia compared to the mako (~20 rows) (Carey et al., 1985). However, another factor affecting lamnid heat conservation is the potential for thermal conductance from red muscle through the surrounding white muscle to the body surface where it would be lost to the ambient water (Graham et al., 1983; Bernal et al., 2003). As shown in Figure 6B, the bulk of the salmon shark's red muscle is confined to its thicker, spindle-shaped mid-body region. Similarly, the axial MR image of the salmon shark shows that its red muscle occurs at a deeper relative position in the body than in the mako. By contrast, the thinner body of the mako also lessens the relative distance between red muscle and the body surface. Additionally, a significant portion of the mako's red muscle extends into the thin, tapering region of the posterior body where it is closer to the body surface.

Elucidation of anatomical detail by careful dissection requires considerable time and usually results in the nearly complete destruction of the specimens examined, largely precluding work on rare or valuable material. Additionally, dissections seldom offer the possibility of reconstructing the specimen to visualize basic design features in their intact, 3D state. This is particularly important for relatively rare or difficult to obtain specimens such as the salmon shark, where the number of samples available for study is very limited. Determining the volumes of organs, muscles, and other tissues by conventional means can be prone to error as well, because of the difficulties associated with physical separation of tissues of interest (e.g., red and white muscle). While digital imaging of the transverse serial sections of a specimen (Bernal et al., 2003) streamlines the acquisition of red muscle and other axial morphological information, sectioning the specimen destroys it and can introduce distortions because of shear and tearing. Further, errors associated with analysis of digitized images result from distortions due to the camera lens or orientation of the object relative to the camera, and are very difficult to quantify. The resolution of data from previous dissection-based measurements (Graham et al., 1983; Carey et al., 1985; Graham and Dickson, 2001; Bernal et al., 2003; Sepulveda et al., 2005) was also limited by the thickness (ca. 2–3 cm) of the transverse body sections, which exceed by at least 30 times the slices resolved by MRI. In contrast to conventional dissection followed by coarse mathematical inter-

polation, MRI offers the fine-scale measurement and 3D analysis of structure geometries and spatial configuration required for understanding many in vivo functions (Donley et al., 2004, 2005; Shadwick, 2005; Hodgson et al., 2006).

The quantitative measurements reported in this study are subject to error due to the effect of "partial voluming" (Thacker et al., 2004), where two different tissues occupy the same image volume element (voxel), resulting in an image intensity intermediate to that of two tissues, depending upon the volume fraction of each. In the present study, the errors in the volume measurements from this effect are relatively small, as the number of voxels representing red muscle volumes is much greater than the voxels representing the non-red muscle border regions. In studies where this effect may be important, two methods for reducing these errors can be employed: acquiring higher resolution data (at the cost of increased imaging time) or direct measurement of the different voxel tissue components (Alfano et al., 1997). The condition of the specimen can also be a source of error. Ideally, fresh specimens would be used, but this is often not possible. Freezing and repeated freeze-thaw cycles can alter tissue microstructure, thereby changing T_1s and potentially reducing contrast. Similarly, chemical preservation with formalin and isopropanol can alter T_1s and thus tissue contrast (Yong-Hing et al., 2005).

In summary, this study demonstrates the efficacy of MRI in conjunction with image and segmentation analyses in providing a synoptic visualization of the intact structure of shark myotomes and related morphological features, such as the hypaxial lateral tendon in the salmon shark, which had not been previously described. MRI is especially important in cases where the post-hoc manipulations of the visual data are needed to enhance interpretation, and this was done in our evaluations of red muscle quantity and position in the salmon and mako sharks. In addition to ensuring the conservation of valued specimens, the storage of digital MRI data will allow multiple intra- and interspecific comparisons.

ACKNOWLEDGMENTS

DPC was supported by a fellowship from UCSD Alliance for Graduate Education and the Professoriate (AGEP) and by a CA Sea Grant traineeship. We thank R. Shadwick and anonymous reviewers for constructive criticisms on this manuscript.

LITERATURE CITED

Alfano B, Arturo B, Covelli E, Quarentelli M, Panico M, Ciarmiello A, Salvatore M. 1997. Unsupervised, automated segmentation of the normal brain using a multispectral relaxometric magnetic resonance approach. Magn Reson Med 37:84–93.

Anderson SD, Goldman KJ. 2001. Temperature measurements from salmon sharks, *Lamna ditropis*, in Alaskan waters. Copeia 2001:794–796.

Bernal D, Dickson KA, Shadwick RE, Graham JB. 2001a. Review: Analysis of the evolutionary convergence for high performance swimming in lamnid sharks and tunas. Comp Biochem Physiol A Mol Integr Physiol 129:695–726.

Bernal D, Sepulveda C, Graham JB. 2001b. Water-tunnel studies of heat balance in swimming mako sharks. J Exp Biol 204: 4043–4054.

Bernal D, Sepulveda C, Mathieu-Costello O, Graham JB. 2003. Comparative studies of high performance swimming in sharks. I. Red muscle morphometrics, vascularization, and ultrastructure. J Exp Biol 206:2831–2843.

Bernal D, Donley JM, Shadwick RE, Syme DA. 2005. Mammal-like muscles power swimming in a cold-water shark. Nature 437:1339–1352.

Bone Q. 1978. Locomotor muscle. In: Hoar WS, Randall DJ, editors. Fish Physiology. New York: Aacademic Press. pp 361–417

Bonney JM, Zanca M, Boepspflug-Tanguy O, Dedieu V, Joandel S, Renou JP. 1998. Characterization in vivo of muscle fiber types by magnetic resonance imaging. Magn Reson Imaging 16:167–173.

Carey FG, Teal JM. 1969. Mako and porbeagle: Warm-bodied sharks. Comp Biochem Physiol 28:199–204.

Carey FG, Teal JM, Kanwisher JW, Lawson KD. 1971. Warm bodied fish. Am Zool 11:135–145.

Carey FG, Casey JG, Pratt HL, Urquhart D, McCosker JE. 1985. Temperature, heat production and heat exchange in lamnid sharks. Mem S Calif Acad Sci 9:92–108.

Compagno LJV. 2001. Sharks of the world. An annotated and illustrated catalogue of shark species known to date. Bullhead, mackerel and carpet sharks (Heterodontiformes, Lamniformes and Orectolobiformes). FAO species catalogue for fishery purposes. No. 1, Vol 2. Rome: FAO. p 269.

Donley JM, Sepulveda CA, Konstantinidis P, Gemballa S, Shadwick RE. 2004. Convergent evolution in mechanical design of lamnid sharks and tunas. Nature 429:61–65.

Donley JM, Shadwick RE, Sepulveda CA, Konstantinidis P, Gemballa S. 2005. Patterns of red muscle strain/activation and body kinematics during steady swimming in a lamnid shark, the shortfin mako (*Isurus oxyrinchus*). J Exp Biol 208:2377–2387.

Ebert DA. 2003. Sharks, rays and chimaeras of California. Berkeley, California: University of California Press.

Ellerby DJ, Altringham JD, Williams T, Block BA. 2000. Slow muscle function of Pacific bonito (*Sarda chiliensis*) during steady swimming. J Exp Biol 203:2001–2013.

Frank LR. 2002. Magnetic resonance imaging: Basic principals. In: Resnick D, editor. Diagnosis of Bone and Joint Disorders. Philadelphia, PA: WB Saunders, pp 72–109.

Goldman KJ, Musick JA. 2006. Growth and maturity of salmon sharks (*Lamna ditropis*) in the eastern and western North Pacific, and comments on back-calculation methods. Fish Bull 104:278–292.

Graham JB, Dickson KA. 2001. Morphological and physiological specializations for endothermy. In: Block BA, Stevens ED, editors. Tuna, Physiological Ecology and Evolution. San Diego: Academic Press. pp 121–165.

Graham JB, Dickson KA. 2004. Tuna comparative physiology. J Exp Biol 207:4015–4024.

Graham JB, Koehrn FJ, Dickson KA. 1983. Distribution and relative proportions of red muscle in scombrid fishes: Consequences of body size and relationships to locomotion and endothermy. Can J Zool 61:2087–2096.

Hodgson JA, Finni T, Lai AM, Edgerton VR, Sinha S. 2006. Influence of structure on the tissue dynamics of the human soleus muscle observed in MRI studies during isometric contractions. J Morphol 267:584–601.

Kirschner-Hermanns R, Fielding JR, Versi E, Resnick NM. 1997. Magnetic resonance imaging of the lower urinary tract. Curr Opin Obstet Gynecol 9:317–319.

Kohler NE, Casey JG, Turner AT. 1996. Length-length and length-weight relationships for 13 shark species from the Western North Atlantic. NOAA Tech Memo NMFS-NE-110.

Mollet HF, Cliff G, Pratt HL, Stevens JD. 2000. Reproductive biology of the female shortfin mako, *Isurus oxyrinchus* Rafinesque, 1810, with comments on the embryonic development of lamnoids. Fish Bull 98:299–318.

Sepulveda CA, Wegner NC, Bernal D, Graham JB. 2005. The red muscle morphology of the thresher sharks (family Alopiidae). J Exp Biol 208:4255–4261.

Shadwick RE. 2005. How tunas and lamnid sharks swim: An evolutionary convergence. Am Sci 93:524–531.

Shadwick RE, Katz SL, Korsmeyer KE, Knower T, Covell JW. 1999. Muscle dynamics in skipjack tuna: Timing of red muscle shortening in relation to activation and body curvature during steady swimming. J Exp Biol 202:2139–2150.

Thacker NA, Williamson DC, Pokric M. 2004. Voxel based analysis of tissue volume from MRI data. Br J Radiol 77:114–125.

Waller GNH, Williams SCR, Cookson MJ, Kaldoudi E. 1994. Preliminary analysis of elasmobranch tissue using magnetic resonance imaging. Magn Reson Imaging 12:535–539.

Woodhead HJ, Kemp AF, Blimkie CJR, Briody JN, Duncan CS, Thompson M, Howman-Giles R, Cowell CT. 2001. Measurement of midfemoral shaft geometry: Repeatability and accuracy using magnetic resonance imaging and dual-energy X-ray absorptiometry. J Bone and Miner Res 16:2251–2259.

Yong-Hing CJ, Obenaus A, Stryker R, Tong K, Sarty GE. 2005. Magnetic resonance imaging and mathematical modeling of progressive formalin fixation of the human brain. Magn Reson Med 54:324–332.